JOURNAL OF APPLIED ELECTROCHEMISTRY **27** (1997) 1245–1253

Passivation and depassivation of Monel electrodes in KF.2HF melts in comparison with the behaviour of nickel

S. Y. QIAN, H. DUMONT, B. E. CONWAY

Chemistry Department, University of Ottawa, 10 Marie Curie Street, Ottawa, Ontario K1N 6N5, Canada

Received 2 January 1997; revised 29 April 1997

Commercial fluorine production is conducted from KF.2HF melts at 85 °C in Monel cells that are subject to corrosion. Here we report studies of passivation and depassivation of the Monel in relation to that of Ni, its principal (65 wt %) constituent, by means of cyclic voltammetry and recording of open-circuit potential-relaxation transients. The latter exhibit arrests at characteristic Flade-type potentials and lead to information on the kinetics of passive film breakdown. The role of diffusion processes in such breakdown and film dissolution is evaluated using the rotating disc electrode technique which enables comparisons to be made with the passivation behaviour of the separate main components of Monel, viz. Ni and Cu.

Keywords: *fluorine production, monel alloy, corrosion, passive films, KF.2HF melts*

1. Introduction

The preferred technology for anodic fluorine production is from a KF.2HF melt at 85 °C. Previous literature [1–3], has been directed mainly to electrochemical problems with the cell electrodes themselves, for example, the anode effect and hyperpolarization at the steel cathodes [3]. Additionally, problems in cell operation arise due to accumulation of impurities in the melt from corrosion of the (usually Monel) cell casings and the steel cathodes, especially if they have suffered hydrogen blistering with spallation of flakes into the melt.

The present paper is part of a series of studies [1–4] on the behaviour of electrodes and cells employed in anodic fluorine production. Immediately related work [4] dealt with the comparative aspects of corrosion of the separate Cu and Ni components of the Monel alloy in the KF.2HF melt.

Although Monel alloy, consisting of about 65 wt % Ni and 31.5 wt % Cu, is fairly corrosion resistant, significant quantities of the principal elements of this alloy are, however, found in the industrial melt and arise from corrosion of the construction materials of the cell. Various reports have appeared in the literature on the anodic behaviour of copper and nickel in aqueous and anhydrous HF [5–9], but few results lead to elucidation of mechanisms and kinetics of the dissolution and passivation of Monel alloy in the KF.2HF melt. The present paper provides such information.

2. Experimental details

2.1. *Electrodes, cell and electrolyte*

The essential details of the experimental procedures used were described in previous papers [3, 4]. Briefly, a Monel or nickel hanging-meniscus, rotating electrode (HMRE), an Fe/FeF_2 reference electrode and a carbon anode (supplied by Sers Savoie Carbone, France) were used. The electrolyte was a melt of anhydrous KF.2HF prepared from the 99 + % KF.HF (solid) and 99.9% HF (liquid) by the reaction of $KF.HF + HF \rightarrow KF.2HF$. A cylindrical plexiglass cell was used and mounted in an air-heated oven (85 °C), as in previous work [3, 4].

The Monel and nickel electrodes having apparent areas of 0.503 cm^2 were prepared, respectively, from Monel and nickel rods (purity > 99.5%) supplied by Johnson Matthey Co.

Elemental analysis of Monel (400) was carried out using a Phillips X-ray fluorescence spectrometer. The elements found in the alloy samples included: Ni (63%), Cu (28–34%), Fe, Mn, Cr, Ti in significant amounts while, Mg, Al, Si, Ti, S, Co, P were present only in traces.

2.2. *Measurements and experimental procedures*

Cyclic voltammetry experiments were conducted at scan rates between 2 and 100 $mV\,s^{-1}$ at a freshly polished Monel and comparatively (cf. [4]) at a Ni disc electrode setup in hanging-meniscus electrode configuration; this provided the most reproducible results. Linear sweeps were started at the open-circuit potential of the studied electrode in the melt. The polarization sequences were controlled by an EG&G potentiostat 273.

Following polarization by means of an HA301 potentiostat (Hokuto Denko Co.), potential–relaxation measurements, designed to provide information on breakdown or dissolution of passive films and related Flade potential behaviour [10], were carried out by interrupting currents using a Clare vaccuum

mercury relay (HGJ2MT 51231 E00). The potential, E, against time, t, relaxation transients were recorded digitally by means of a Nicolet oscilloscope (model 310). The resulting $E(t)$ data were processed by an IBM-type PC.

Experiments on the role of diffusion in passivation and corrosion of nickel, were carried out at a rotated nickel disc electrode using a Pine Instrument Company rotator.

3. Results and discussion

3.1. *Cyclic voltammograms for Monel and Ni electrodes in the KF.2HF melt*

The cyclic voltammetry experiments were carried out at Monel electrodes in the KF.2HF melt in the potential range -0.1 to $+3.9$ V vs Fe/FeF_2 as shown in Fig. 1, together with those for Cu and Ni separately recorded. The inset shows the same results but plotted on a more sensitive current scale. The potential at which the peak current arises at Monel is higher than that for the Ni electrode, indicating that oxidative dissolution and fluoride film formation is more difficult, but this peak potential is at the same as that for Cu dissolution [4]. The current required for maintenance of passivation after the latter has set in is, however, much smaller at Monel ($\sim 0.1\,mA\,cm^{-2}$), being less than half of the corresponding current at nickel; see inset in Fig. 1.

At potentials >3 V vs Fe/FeF_2, the current at a Ni becomes significantly increased (Fig. 1) due to fluorine evolution as a transpassive process but a similar effect is not observed at the Monel electrode indicating that fluorine evolution reaction on oxidized Monel requires higher overpotentials for given anodic current densities.

On a cathodic sweep, cathodic reduction currents are not observed at a passivated Monel surface, as also found at the passivated Ni electrode; thus, the passive film on Monel probably consists in part of Ni fluoride, which is irreducible [4] at potentials less negative than that for hydrogen gas evolution.

3.2. *Role of diffusion-control in anodic dissolution of Ni and Monel in the KF.2HF melt*

Figure 2 shows the anodic behaviour of Monel under linear-sweep voltammetry at scan rates (SR) between 2 and $100\,mV\,s^{-1}$, starting at the open-circuit potential of a freshly polished hanging meniscus electrode in the KF.2HF melt. A large anodic current peak, dependent on square-root of sweep-rare (Fig. 2 inset), arises between ~ 0.63 to 0.78 V associated with diffusion-controlled formation and dissolution of the passive film at Monel. Compared with the voltammograms for Ni (Fig. 3), the anodic peak at Monel arises at a higher potential (between 0.24 to 0.42 V) and, being narrower than that at Ni indicates that the passive film at Monel requires less charge for its formation than for Ni. The anodic peak currents at the Ni electrode are also linear in square-root of scan rate (Fig. 3, inset) indicating that the processes at Ni electrodes are also diffusion-controlled.

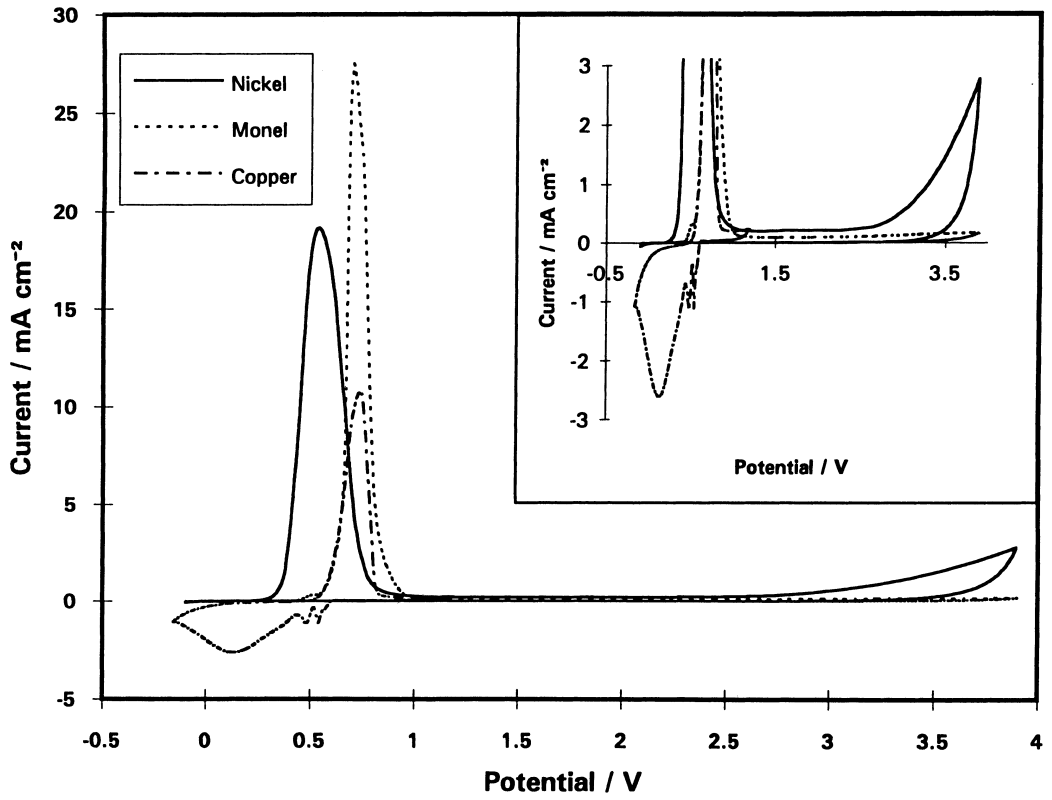

Fig. 1. Comparison of cyclic voltammograms obtained at Cu, Ni and Monel electrodes in the KF.2HF melt at 85 °C. Inset: same results but plotted on a more sensitive current scale.

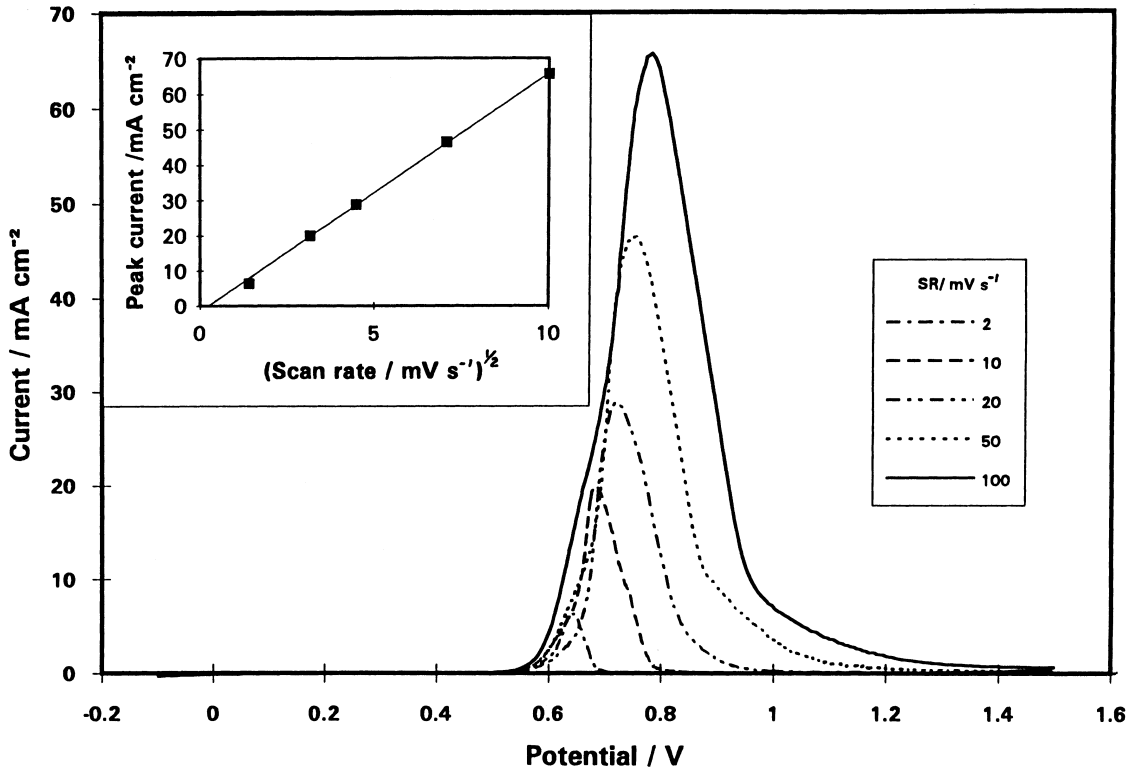

Fig. 2. Effect of scan rate (SR) on the voltammograms obtained for Monel electrodes in the KF.2HF melt at 85 °C. Inset: the I_{peak} against (scan rate)$^{1/2}$ relation for the anodic dissolution peak.

3.3. *Nucleation and growth of NiF_2 films on Ni*

3.3.1. Sweep reversal experiments. The voltammetric behaviour of a freshly polished Ni electrode at successively increasing positive reversal potentials, E_{rev}, was studied. The first anodic scan to 270 mV is shown in Fig. 4 (solid line 1) and its reverse was almost coincident with the anodic one. On the second (dot-

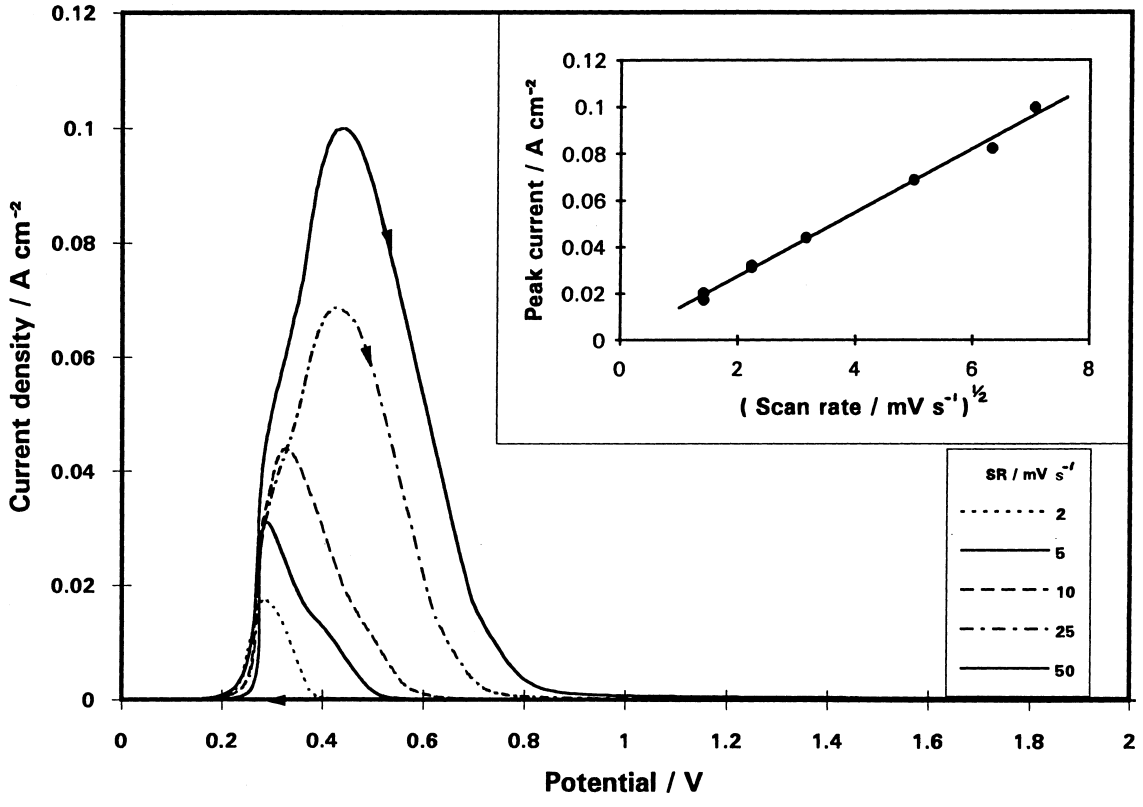

Fig. 3. Effect of scan rate on the voltammograms obtained for Ni electrodes in the KF.2HF melt at 85 °C. Inset: the I_{peak} against (scan rate)$^{1/2}$ relation for the anodic dissolution peak on Ni.

ted line 2) and third cycles, the currents become increased especially on the reverse negative-going scan, becoming larger than on the anodic scan (Fig. 4). This behaviour is typical of a nucleation process leading to an 'autocatalytic' type of electrochemical behaviour [11, 12] and also demonstrates that initial anodic dissolution of Ni is a prerequisite for the onset of nucleation of a film of NiF_2 related to the consumption of previously dissolved Ni cations near the electrode surface.

3.3.2. Potentiostatic current-time transients at a Ni electrode in the KF.2HF melt. Nucleation of NiF_2 was further investigated by studying current transients in response to potential pulses from 0.195 V to a range between 0.280 and 0.370 V as shown in Fig. 5 where potential-dependent increases of current arise after an initial induction time. The resulting experimental line indicates an induction time decreasing with increasing anodic pulse potential.

After an initial dissolution of Ni as Ni^{2+}, the Ni ions (plus excess F^-) reach saturation solubility near the electrode surface, leading to a spontaneous nucleation of NiF_2 with fast growth of nuclei; this then leads locally to rapid removal of Ni ions in the boundary layer and hence to a temporary increase in the local dissolution rate. The latter process becomes slowed after longer times by NiF_2 film formation and eventually passivation sets in by the deposition of NiF_2 arising from the probably supersaturated solution as Ni dissolution is becoming retarded. This final stage of diffusion of NiF_2 leads to a decrease of current according to a Cottrell-type decay. Two diffusion regimes are observed in this decay, one probably being associated initially with the diffusion of Ni ions from the more concentrated region near the surface (fast regime) and later from the bulk of the melt (slow regime), the residual current being the passivation-maintenance current. The passivation-mechanism is thus a complicated process involving competition between diffusion of dissolved Ni ions from the electrode together with the nucleation process. The overall process can be represented schematically by

$$\begin{array}{ccccc} Ni & \longrightarrow & Ni^{2+}_{(surf.)} & \xrightarrow{1} & Ni^{2+}_{(soln.)} \\ & & \text{fast}\ \searrow\ 2 & & \swarrow\ \text{slow} \\ & & & NiF_{2(solid)} & \end{array} \qquad (1)$$

3.3.3. Potentiostatic current-time transients obtained at the hanging-meniscus rotating-disc Ni electrode in the KF.2HF melt. Figure 6 shows the current transients obtained after application of potential pulses from 0.195 V to 0.33 V vs Fe/FeF_2 at different electrode rotation rates. The currents decrease with increasing rotation rate, which is contrary to expected regular diffusion-controlled behaviour (path 1 of Equation 1). The observed behaviour thus suggests that the high anodic current (rate of the anodic process) at the stationary electrode, due to

$$Ni \rightarrow Ni^{2+}_{(surf.)} + 2e^- \qquad (2)$$

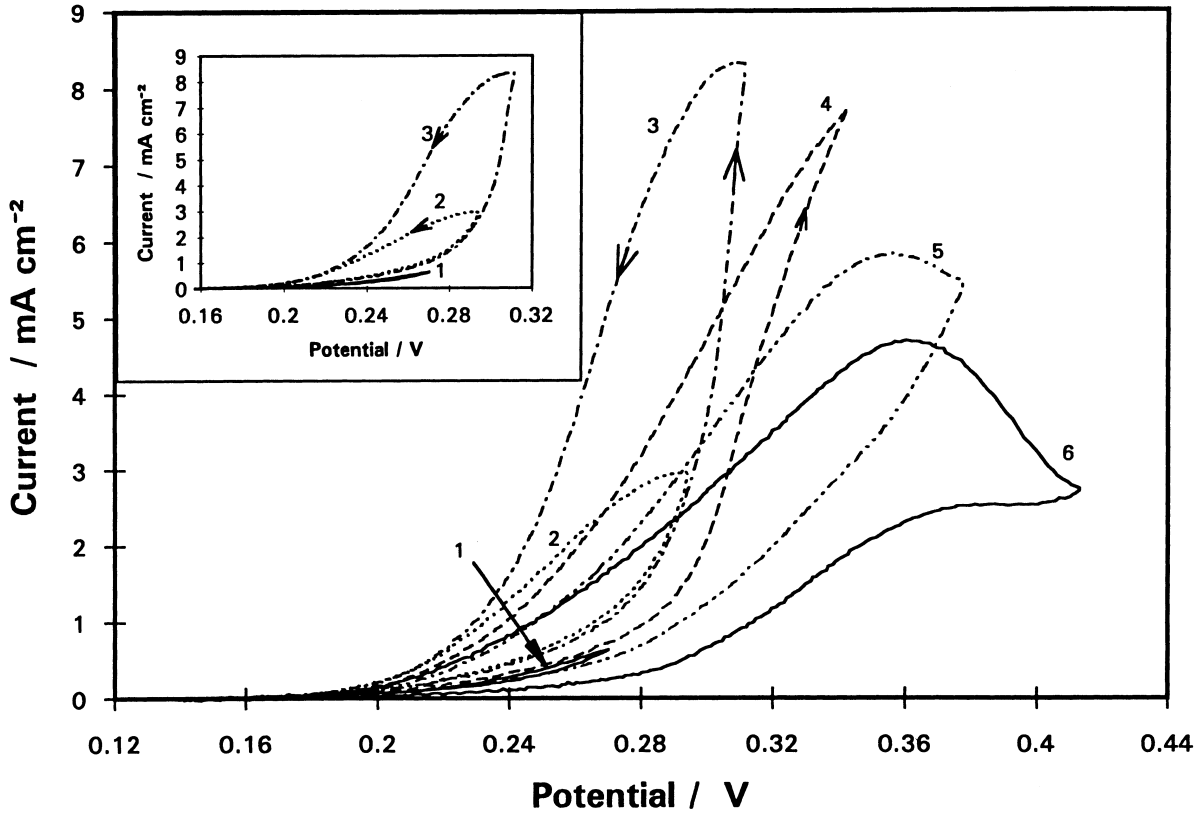

Fig. 4. Cyclic voltammograms for various anodic reversal potentials, E_{rev}, for the Ni electrode in the KF.2HF melt at 85 °C. E_{rev}: (1) 270, (2) 300, (3) 330, (4) 360, (5) 390 and (6) 420 mV. Inset: first three cycles for clarification.

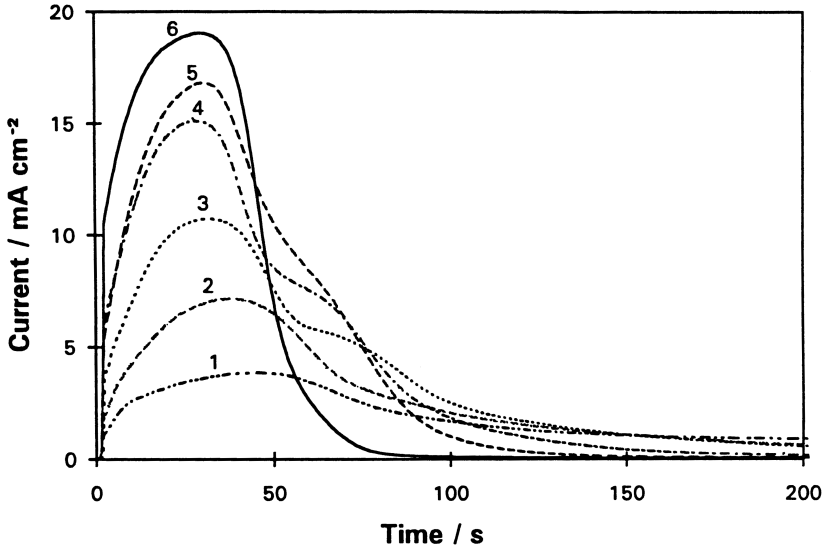

Fig. 5. Potentiostatic current–time transients recorded at Ni after application of potential pulses from $E_{open} = 0.195$ V to (1) 0.28, (2) 0.29, (3) 0.31, (4) 0.33, (5) 0.35 and (6) 0.37 V.

is actually dominated by the nucleation process (path 2 of Equation 1):

$$Ni^{2+}_{(surf.)} \rightarrow NiF_{2(solid)} \quad (3)$$

rather than by diffusion of Ni^{2+} species away from the electrode surface. When the rotation rate is increased, the local concentration of Ni^{2+} at the surface, $C_{(0,t)}$, tends to become reduced, thus diminishing the nucleation and film growth. Since this step dominates the anodic dissolution current, the net current is therefore reduced. Otherwise, if the Ni^{2+} diffusion *from* the electrode surface were the dominant step, increase of the rotation rate would increase the dissolution current, which is not the case. On the other hand, if rotation rates were high enough, the concentration of Ni^{2+} at the electrode surface would not reach saturation (as NiF_2), so that nucleation and film growth would be prevented leading to complete control of the current by mass transfer.

Current transient recordings were also made by applying a given potential pulse at the rotating electrode but with a stepwise change of the rotation rate from 0 to 2500 rpm or from 2500 to 0 rpm in the middle of the transient. The current at 0 rpm became increased to 8.5 mA, but then was reduced to below 2 mA after the electrode was rotated at 2500 rpm. This behaviour is ascribed to reduction of the concentration of $Ni^{2+}_{(surf.)}$ by rotation, referred to above, which thereby slows down the nucleation process, causing the current to become reduced.

When a potential pulse is applied to an electrode rotated at 2500 rpm, the current reaches 1.3 to 2 mA and then becomes reduced. This effect is related to partial blocking of the electrode surface as the nucleation, although less important at this rotation frequency, becomes initiated. After about 50 s, the electrode rotation was stopped and the current then gradually increased which confirms that the electrode

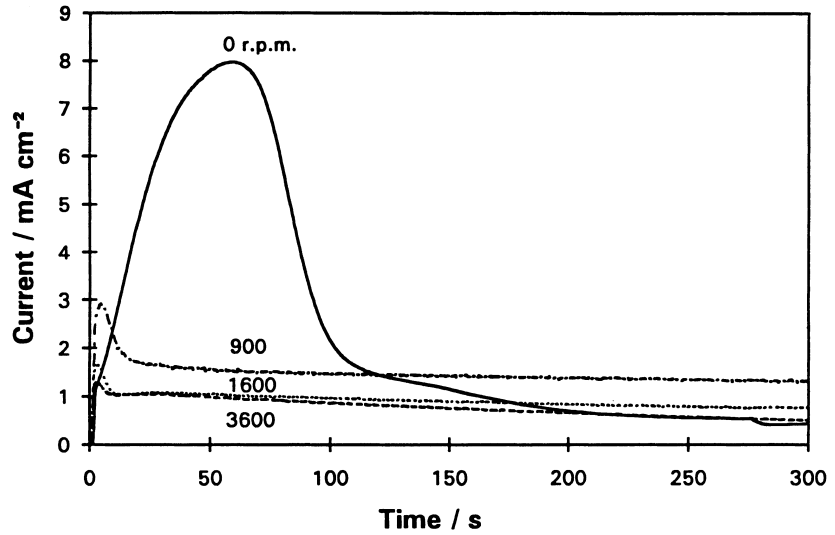

Fig. 6. Potentiostatic current–time transients recorded at various rotation rates at an HMRD Ni electrode after application of a potential pulse from 0.195 V to 0.33 V vs Fe/FeF_2.

is probably partially covered by the passive film, otherwise the current increase should be much larger (as was actually seen at the stationary electrode); in fact, a visible film is formed on the electrode after the potential pulse had been applied at a rotation rate of 2500 rpm.

3.3.4. Open-circuit potential decay. The so-called 'potential-decay' procedure provides a method for following the autodecomposition, and rates thereof, of passive films which leads to information [13] on their previous extent of formation and their mechanisms of breakdown or dissolution. In the present set of experiments, the electrode of interest was first subjected to a potential sweep (20 mV s^{-1}) starting at the corrosion potential (i.e. ~ 0.19 V vs Fe/FeF_2 for the Ni electrodes) and ending at 1 V vs Fe/FeF_2 at which it was held for various times, which will be referred to as 'passivation time'; then the circuit was opened and the potential vs time transient was digitally recorded.

The *potential decay* transient is generally composed of three distinguishable sections (Fig. 7). First an exponential potential decrease arises associated with discharge of the double-layer capacitance followed by a later relaxation due to discharge of any adsorption-capacitance [14] (Fig. 7, region a), This discharge time (mostly pseudocapacitance discharge) is called here the self-activated discharge ('depassivation') time and is proportional to the charge (film thickness) for previous film formation. It can be used to determine the fluoride film-growth law by determining self-discharge times following previous anodic polarizations for various durations corresponding to growth of the passive film. After the self-depassivation, the potential vs time transient exhibits an intermediate arrest at a Flade potential [10]. After this transistion time the potential drops rapidly (Fig. 7, region b) to the final plateau (region c) and then gradually approaches the natural corrosion potential.

Oxide film growth at metals usually follows either a so-called 'direct' or 'inverse' logarithmic law in time [15]. We expect such relations also to apply to growth of passivating fluoride films. For the inverse law, Mott and Cabrera [16–19] deduced:

$$q^{-1} \propto \log(t/d^2) \tag{4}$$

where q is the charge for film formation to a thickness, d.

On the other hand, the direct law is [16]:

$$\frac{dq}{dt} = k\exp(-Lq) \tag{5}$$

which integrates to

$$q = \frac{1}{L}\ln kL + \frac{1}{L}\ln\left[t + \frac{\exp(Lq_0)}{kL}\right] \tag{6}$$

where q_0 is proportional to the extent of any prior film formation at $t = 0$. When $t \gg \{\exp(Lq_o)\}/kL$, q, that is, the extent of film formation, will be linear to $\log t$.

The dissolution time at Ni (determined by film thickness) is perfectly linear in the log of the previous time of anodic passivation (Fig. 7 inset) indicating that the film growth at Ni follows the direct logarithmic law. Its slope is determined by the rate of film thickening.

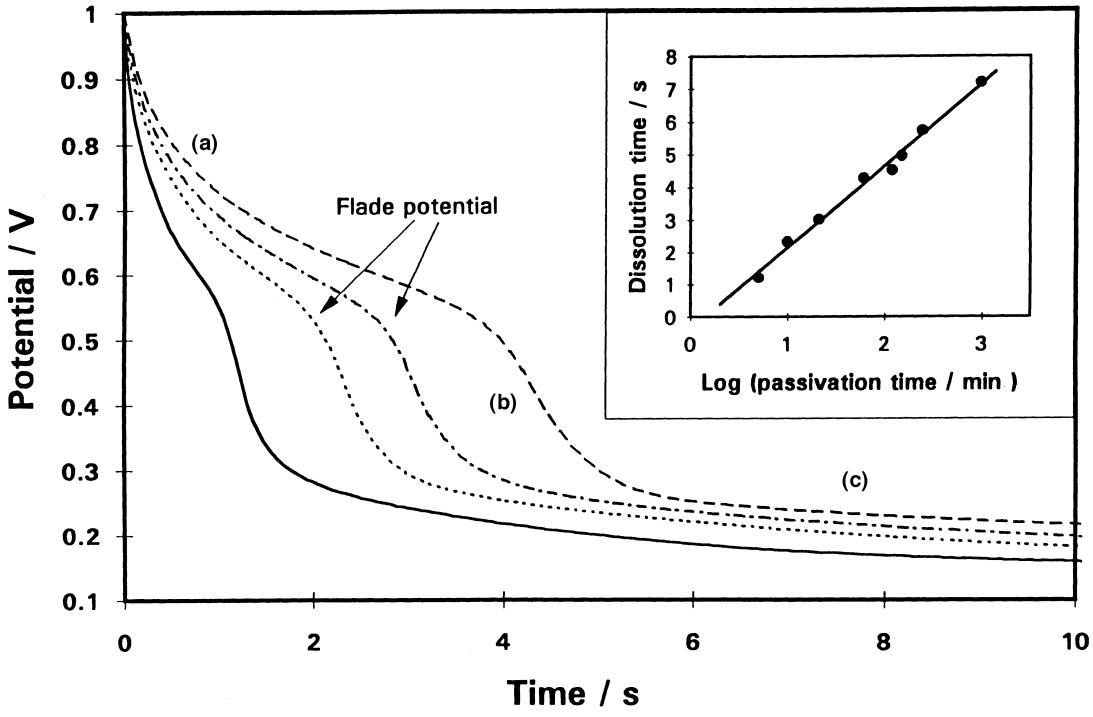

Fig. 7. Open-circuit potential decay transients at Ni electrodes in the KF.2HF melt after passivation at 1 V vs Fe/FeF_2 for (———) 5, (· · · · ·) 10, (– · – · –) 21 and (– – ––) 60 min. (a) Self-discharge region; (b) sudden potential drop to E_{corr} plateau; (c) approach to corrosion potential. Inset: the dissolution time against log of previous passivation time for NiF_2 film formation in KF.2HF melt.

3.4. *Dissolution and passivation of Monel*

3.4.1. Sweep reversal experiment. Figure 8 shows the voltammetric responses at $5\,mV\,s^{-1}$ of a Monel electrode at successively increasing positive reversal potentials and its inset the behaviour on a more sensitive current scale. Currents become decreased as the electrode is scanned anodically to 0.57 V, then scanned back negatively (compare Fig. 4 for Ni). A cathodic reduction current is observed at the Monel electrode, like that at Cu [4]. When the anodic sweep reversal potential, E_{rev}, was increased to 0.6 V, the cathodic current became bigger indicating that: (a) the nucleation and film growth observed on Ni is not effective in the passivation of Monel and (b) reduction reaction peaks are observed due to anodically dissolved Cu^{2+} that become reduced (cf. [4]) around 0.48 V vs Fe/FeF_2 (Fig. 8). When E_{rev} was further increased, passivation set in at ~ 0.68 V and the current became negligible. Then no reduction current is observable on the negative-going sweep (see dashed line in Fig. 8).

3.4.2. Open-circuit potential-decay behaviour at Monel electrodes passivated at 2 V in the KF.2HF melt. Open-circuit potential decay experiments were carried out at Monel electrodes, comparatively vis-a-vis Ni, held at 2 V vs Fe/FeF_2 for various times after application of potential sweeps at 20 mV s^{-1}, starting at the corrosion potential as shown in Fig. 9. The curves are still composed of three distinguishable sections, as in the case of Ni. The potentials at which the curves have sharp inflections are coincident with the potentials at which the dissolution and passivation appears in the cyclic voltammogram (Fig. 2). The depassivation time is now non-linear in the log of previous passivation (holding) time, so that the direct logarithmic law, observed at Ni, is *not followed.* However, when the reciprocal of the depassivation time was plotted against the log of passivation time (Fig. 9, inset), a good linear relation resulted indicating that the 'inverse' logarithmic law [19] is now applicable. Oxide films grow by formation and injection of ions from the metal surface across an interfacial energy barrier, into interstitial positions in the growing oxide phase, followed by field-assisted transport through the oxide layer. The present results in the melt suggest that a similar mechanism applies to fluoride film growth at Monel. The applicability of the 'inverse' logarithmic law to fluoride film growth at Monel is related to the poor conductivity of copper fluoride when in the passive film.

3.4.3. Hydrogen evolution and oxygen reduction involved in the dissolution and passivation behaviour at Monel electrodes in the KF.2HF melt. Figure 10 shows the potential vs current diagram obtained for corrosion of the Monel electrode after it had been immersed in the KF.2HF melt for 742 h. For comparison the curves obtained at Ni and Cu electrodes are also plotted on this diagram (here for the purpose of comparison between the potential ranges involved). The corrosion potential for Monel alloy itself is located at ~ 0.48 V vs Fe/FeF_2 (exactly the

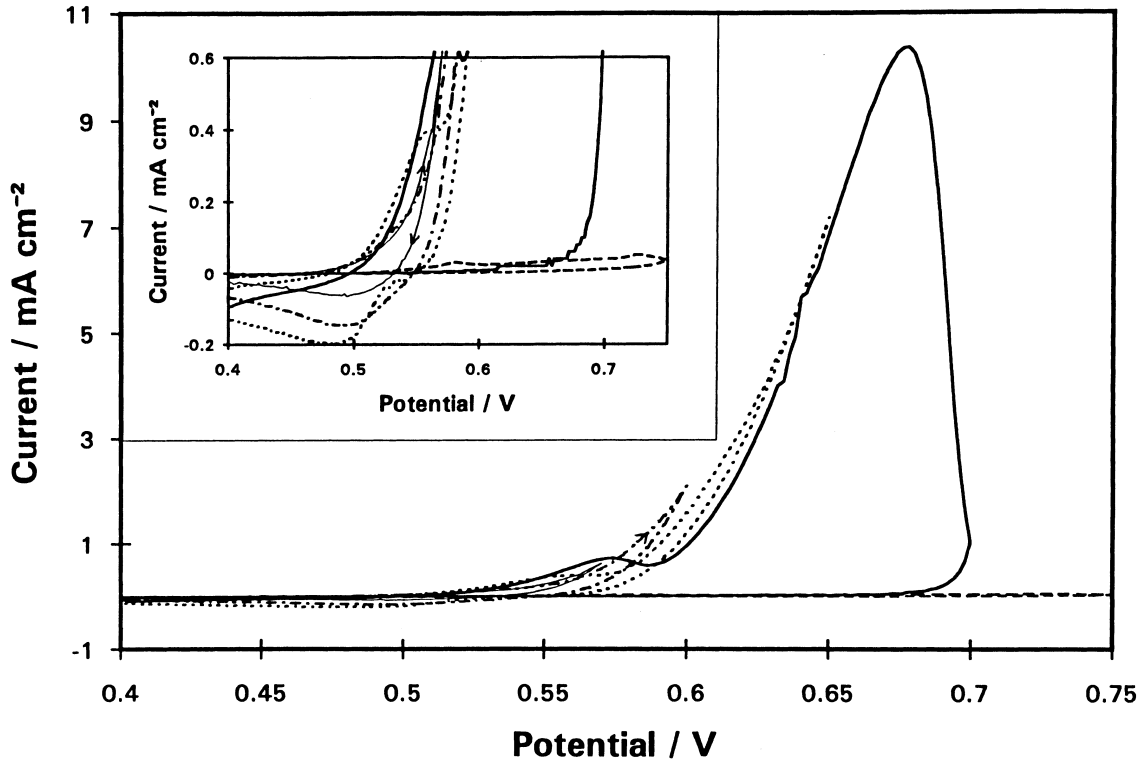

Fig. 8. Cyclic voltammograms taken from different anodic reversal potentials, E_{rev}, for the Monel electrode in the KF.2HF melt at 85 °C. $E_{rev.}$: (———) 0.57, (– · – · –·) 0.6, (· · · · ·) 0.65, (———) 0.7 and (– – ––) 0.75 V. Inset: same results but plotted on a more sensitive current scale.

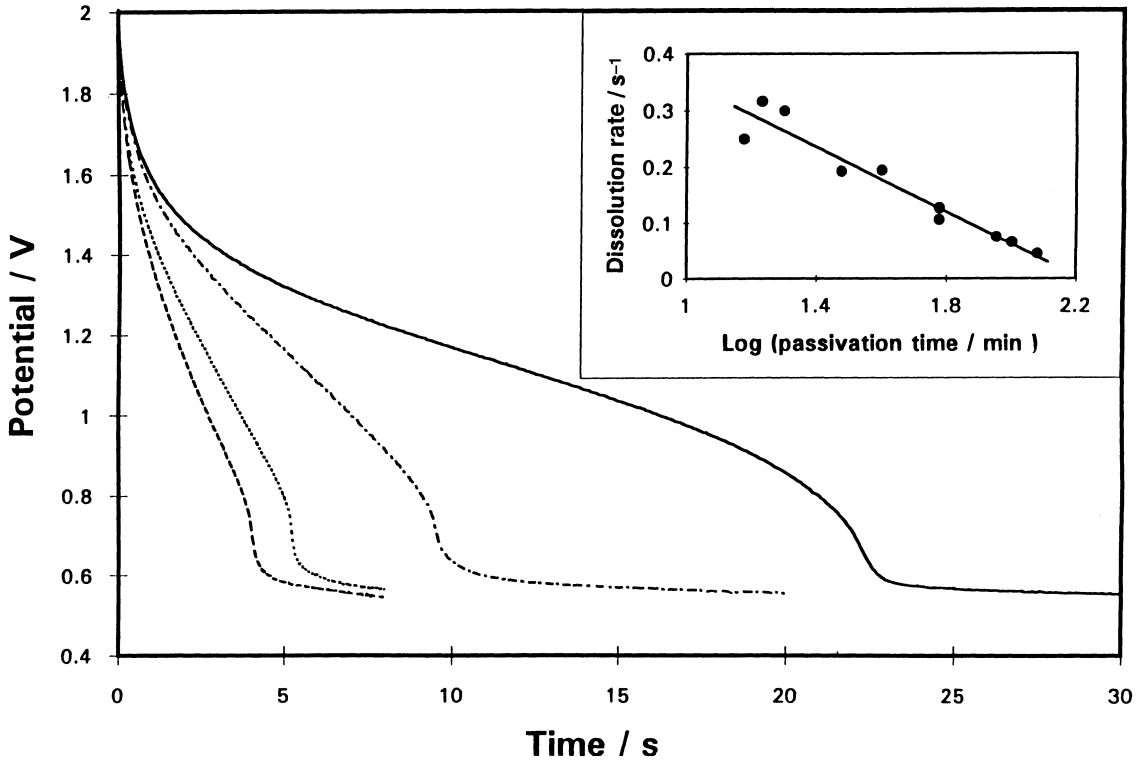

Fig. 9. Open-circuit potential decay transient at a Monel electrode after various times of passivation at 2 V vs Fe/FeF_2 in the KF.2HF melt at 85 °C. Passivation time: (– – ––) 15, (· · · · ·) 30, (– · – · –·) 60 and (———) 120 min. Inset: the reciprocal of the dissolution rate vs log of passivation time for passive film formation at Monel.

same potential as that for a Cu electrode) while for a Ni electrode it is about 0.2 V. Clearly the element Ni on/in the surface of the Monel electrode has been passivated at this potential (Ni passivation sets in at ~ 0.3 V vs Fe/FeF_2, see Fig. 3). The hydrogen evolution potential is about 0.1 V on the same scale. The cathodic branch of the Monel polarization curve clearly exhibits two slopes: below 0.1 V it must correspond to cathodic H evolution while above 0.15 V cathodic reduction of atmospheric oxygen that has entered the cell is dominant. The overall corrosion rate in this case is limited by the rate of oxygen reduction; if the latter could be diminished, the rate of corrosion of Monel would be reduced significantly because the anodic reaction would have to be driven to the mixed potential for the hydrogen reaction for which the current would be much smaller (see point A in Fig. 10).

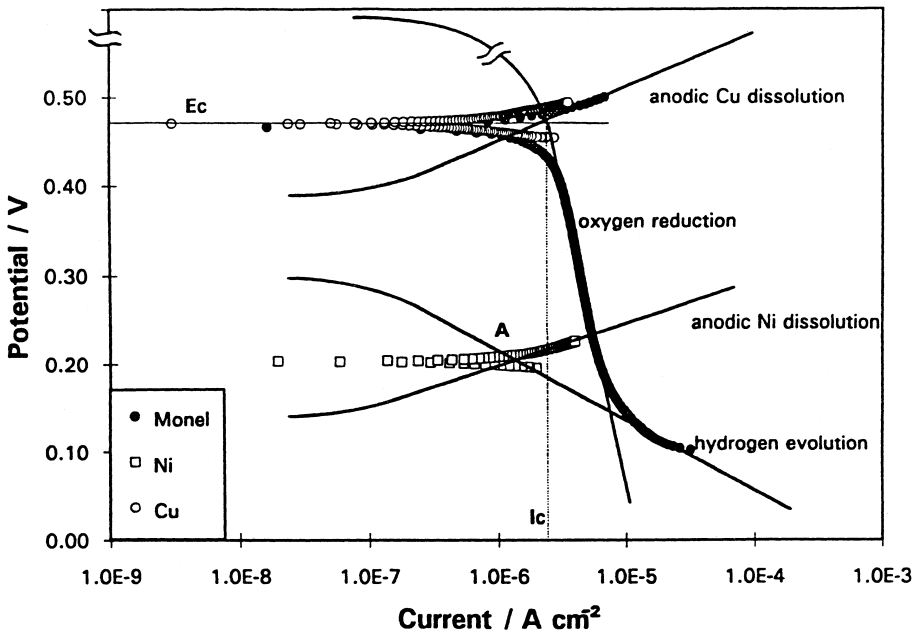

Fig. 10. Schematic mixed-process polarization diagram (solid lines) for corrosion of Monel, and for Cu and Ni in the KF.2HF melt. The symbols represent the experimental data.

3.5. *Comparison of the dissolution and passivation behaviour of Ni and Monel*

The anodic dissolution peak current at Monel arises at a potential higher than that at Ni, but is exactly at the same potential as that for Cu dissolution, indicating that the reaction of dissolution and passivation on Monel is related to the behaviour of its Cu component. The passivation maintenance current after the electrode has become passivated is, however, much smaller at Monel. It was shown earlier in this paper that a nucleation process is involved in the dissolution and passivation of the Ni, but, surprisingly, such behaviour is not observed on the Monel electrode.

A cathodic reduction current can be observed at the Monel electrode on the negative-going sweep before the passive film is formed. It probably arises due to the presence of anodically dissolved Cu^{2+} species that can be easily reduced in the cathodic sweep as was found in our previous studies on Cu corrosion in the fluoride melt [4]. However, after passivation of Monel, no cathodic reduction currents are observed, as was also found at Ni. Thus, it seems that the passive film on Monel consists significantly of Ni fluoride, which is very difficult to reduce in a negative-going potential sweep (cf. [4]).

4. Conclusions

(i) Anodic dissolution of Monel and nickel is controlled by a diffusion step, prior to passivation.
(ii) The fluoride film that causes passivation at Monel or Ni is irreducible at potentials less than that for hydrogen evolution.
(iii) A nucleation process is involved in the dissolution and passivation of nickel. The thickness of the passivating fluoride film at nickel increases linearly with the log of the polarization time. The results enable a mechanism for anodic dissolution and passivation of Ni in the KF.2HF melt to be proposed.
(iv) Before formation of a passive film, a cathodic reduction current can be observed at Monel probably owing to the generation of dissolved Cu^{2+} species which are reducible in the cathodic sweep. However, after passivation has set in, no cathodic reduction current can be observed; this arises because the passive film consists, in part, of NiF_2 which is irreducible and thus provides 'anodic protection' of Monel to corrosion. The growth of the passive film at Monel follows the 'inverse' logarithmic law.

Acknowledgements

Grateful acknowledgement is made to Cameco Corporation, Canada and the Natural Sciences and Engineering Research Council of Canada for financial support of this work. Special thanks are due to Dr D. G. Garratt of Cameco Corp. for many useful discussions.

References

[1] L. Bai and B. E. Conway, *J. Appl Electrochem.* **18** (1988) 839.
[2] L. Bai and B. E. Conway, *ibid.* **20** (1990) 925.
[3] S. Y. Qian and B. E. Conway, *ibid.* **24** (1994) 195.
[4] H. Dumont, S. Y. Qian and B. E. Conway, *ibid.* **27** (1997) 267.
[5] N. Hackerman, E. S. Snavely, Jr. and L. D. Fiel, *Electrochim. Acta* **12** (1967) 535.
[6] M. Cid, A. Jouanneau, D. Nganga and M. C. Petit, *ibid.* **23** (1978) 945.
[7] B. Löchel, H. -H. Strehblow and M. Sakashita, *J. Electrochem. Soc.* **131** (1984) 522.
[8] J. S. Clarke and A. T. Kuhn, *J. Electroanal. Chem.* **85** (1977) 299.
[9] S. Virtanen, H. Wojtas, P. Schmuki and H. Böhni, *J. Electrochem. Soc.* **140** (1993) 2786.
[10] F. Flade, *Z. Phys. chem.* **76** (1911) 503.
[11] P. J. Sonneveld, W. Visscher and E. Barendrecht, *Electrochim. Acta* **37** (1992) 1199.
[12] D. W. Shoeshith, T. D. Rummery, D. Owen and W. Lee, *J. Electrochem. Soc.* **123** (1976) 790.
[13] R. L. Brossard, *Can J. Chem.* **60** (1982) 616.
[14] D. A. Harrington and B. E. Conway, *J. Electroanal. Chem.* **221** (1987) 1–21.
[15] B. E. Conway, B. Barnett, H. Angerstein-Kozlowska and B. V. Tilak, *J. Chem. Phys.* **93** (1990) 8361.
[16] N. F. Mott, *Trans. Faraday Soc.* **35** (1939) 1175.
[17] *Idem*, *ibid.* **36** (1940) 472.
[18] *Idem*, *ibid.* **43** (1947) 429.
[19] N. Cabrera and N. F Mott, *Rep. Prog. Phys.* **12** (1949) 163.